สำนักงานวิทยทรัพยากร
จุฬาลงกรณ์มหาวิทยาลัย

CHAPTER IV
INFLUENCE OF MOLECULAR CHARACTERISTICS ON OVERALL ISOTHERMAL MELT-CRYSTALLIZATION BEHAVIOR AND EQUILIBRIUM MELTING TEMPERATURE OF SYNDIOTACTIC POLYPROPYLENE

4.1 Abstract

Overall isothermal melt-crystallization and subsequent melting behavior of metallocene-catalyzed syndiotactic polypropylene resins of various molecular weights were investigated using differential scanning calorimetry (DSC) technique. Two sets of molecular weight range were synthesized with two different metallocene catalyst systems. The kinetics of the overall isothermal melt-crystallization process was analyzed based on various macrokinetic models, i.e. the Avrami, Malkin and Urbanovici–Segal models. The effective activation energy describing the overall isothermal crystallization process over the crystallization temperature range studied was estimated based on an Arrhenius approximation of the obtained Avrami crystallization rate constants. The equilibrium melting temperature for each of these resins was estimated based on the linear and non-linear Hoffman–Weeks extrapolative methods.

4.2 Introduction

After Ziegler–Natta catalyst had been introduced in the middle of 1950s, the isotactic form of polypropylene (iPP) was successfully synthesized in 1958.Two years later, the syndiotactic form of the same polymer was successfully synthesized [1,2] using the same type of catalyst system, but the resulting polymer contained a considerable amount of both stereo- and regio-irregular defects. In 1988, production of highly stereo- and regio-regular sPP was realized with the advent of the metallocene catalyst system [3]. This led to a renewed interest on this polymer.Some prospective uses for sPP in the industries are, for examples, in film [4,5], injection molding [6], and melt-spun fiber [7,8] applications.

It is generally known that physical and mechanical properties of a semi-crystalline polymer are dictated by morphology, which, in turn, is influenced by crystallization behavior of the polymer. Crystallization behavior is strongly influenced by molecular characteristics (e.g. molecular weight averages, molecular weight distribution, stereo-regularity, etc.) of the crystallizing polymer and the processing conditions. It is, therefore, of our interest to study the effects of molecular characteristics on crystallization kinetics of a semi-crystalline polymer, which is a key to determine the final properties of a polymeric product.

In the present contribution, a differential scanning calorimeter (DSC) is used to study the overall isothermal melt-crystallization and subsequent melting behavior of sPP resins of various molecular characteristics. The crystallization isotherms were analyzed based on the Avrami, Malkin, and Urbanovici–Segal macrokinetic models. The effective activation energy for describing the overall isothermal melt-crystallization process was estimated based on an Arrhenius approximation of the obtained Avrami crystallization rate constants. Finally, the equilibrium melting temperature for each of these resins was estimated according to the linear and nonlinear Hoffman–Weeks extrapolative methods.

4.3 Theoretical Background

The Avrami model [9–11] is the most common approach for describing the kinetics of crystallization process. In order to describe the overall isothermal crystallization kinetics of a semi-crystalline polymer, the Avrami equation is expressed as

$$\theta(t) = 1 - \exp\left[-(K_A t)^{n_A}\right], \tag{4.1}$$

where $\theta(t)$ is the time-dependent relative crystallinity function, K_A is the Avrami rate constant, and n_A is the Avrami exponent.Usually, K_A is written in the form of a composite Avrami rate constant ka (i.e. $k_A = K_A^{n_A}$).Use of K_A is more preferable, since

its units are inverse time. Despite its popularity, the Avrami model is often thought to be appropriate in describing only in the early stages of the crystallization process. The complications arise due to the effects of growth site impingement and secondary crystallization process, which occur in the later stages of the crystallization process.

The time-dependent relative crystallinity function $\theta(t)$ is the fractional crystallinity at a specific time divided by the fractional crystallinity obtained over the whole crystallization period. Since crystallization is exothermic, it is assumed that the fractional crystallinity is linearly proportional to the enthalpy released during the crystallization process. This notion allows for the $\theta(t)$ function to be determined from the ratio of the integral of the enthalpy of crystallization over an arbitrary crystallization period to the integral of the enthalpy of crystallization over the overall crystallization period, i.e.

$$\theta(t) = \frac{\int_0^{t'} (\mathrm{d}H_c/\mathrm{d}t')\mathrm{d}t'}{\Delta H_c}, \tag{4.2}$$

where $\mathrm{d}H_c$ is the instantaneous enthalpy of crystallization released at an arbitrary crystallization time and ΔH_c is the enthalpy of crystallization released over the course of crystallization period.

Malkin et al.[12] proposed a macrokinetic equation based on a postulation that the overall crystallization rate equals the summation of the rate at which the degree of crystallinity varies with the emergence of the primary nuclei and the rate of variation in the degree of crystallinity varies with the crystal growth rate. Mathematically, they arrived at an equation of the form:

$$\theta(t) = 1 - \frac{C_0 + 1}{C_0 + \exp(C_1 t)}, \tag{4.3}$$

where C_0 is the Malkin exponent which relates directly to the ratio of the crystal growth rate G to the primary nucleation rate I (i.e. $C_0 \propto G/I$) and C_1 is the Malkin rate constant which relates directly to overall crystallization rate (i.e. $C_1 = aG + bI$, where a and b are specific constants).It should be noted that the units of C_1 are inverse time.

Urbanovici and Segal [13] modified the Avrami model and proposed a new kinetic equation in the following form:

$$\theta(t) = 1 - \left[1 + (r-1)(K_{US}t)^{n_{US}}\right]^{1/(1-r)}, \tag{4.4}$$

where K_{US} and n_{US} are the Urbanovici–Segal rate constant and the Urbanovici–Segal exponent, respectively, and r is a parameter which satisfies the condition $r > 0$. When the value of r approaches 1, the Urbanovici–Segal equation becomes identical to the Avrami equation. This simply means that the parameter r is merely a factor determining the degree of deviation of the Urbanovici–Segal model from the Avrami model. It is noted that the Urbanovici–Segal kinetic parameters (i.e. K_{US} and n_{US}) have a similar physical meaning to the Avrami kinetic parameters (i.e. K_A and n_A) and the units of K_{US} are, again, inverse time.

The equilibrium melting temperature T_m^0 is an important thermodynamic parameter for determining the degree of undercooling, which signifies the kinetic driving force for crystallization of a crystallizable polymer. It is simply said that no crystallization can occur at temperatures greater than the T_m^0. Theoretically, T_m^0 is defined as the melting temperature of an infinitely large stack of extended-chain crystals in the directions perpendicular to the chain axis and with the chain ends establishing an equilibrium state of pairing [14].

Hoffman and Weeks [15] proposed a method for determining the T_m^0 which states a finite linear relationship between the observed melting temperature T_m and the crystallization temperature T_c according to the following equation:

$$T_m = \frac{T_c}{2\beta} + T_m^0\left[1 - \frac{1}{2\beta}\right], \tag{4.5}$$

where β is the ratio of the thickness of the mature crystals to that of the initial ones or the thickening ratio. β bares a value greater or equal to 1. Due to the suggested linearity of the T_m–T_c data in Eq.(4.5), this approach will be referred to as the linear Hoffman–Weeks extrapolative method (LHW).

Recently, Marand et al.[14] proposed a new mathematical derivation that states a relationship between the observed T_m and the corresponding T_c, by considering the possibility for the stem length fluctuation during secondary nucleation.The new equation reads

$$\frac{T_m^0}{T_m^0 - T_m} = \beta^m \frac{\sigma_e^1}{\sigma_e^{GT}}\left[\frac{T_m^0}{T_m^0 - T_c} + \frac{D_2 \Delta H_f^0}{2\sigma_e^1}\right], \tag{4.6}$$

where β^m is the thickening coefficient, σ_e^{GT} is the basal interfacial free energy associated with nuclei of critical size including the extra lateral surface energy due to fold protrusion and the mixing entropy associated with stems of different lengths, σ_e^1 is the interfacial energy associated with the formation of the basal plane of the initial crystals, D_2 is an arbitrary constant, and ΔH_f^0 is the equilibrium enthalpy of fusion. Due to the suggested non-linearity of the T_m–T_c data in Eq.(4.6), this approach will be referred to as the non-linear Hoffman–Weeks extrapolative method (NLHW).

4.4 Experimental

4.4.1 Materials

Six sPP resins (i.e. internal codes: sPP#9 to sPP#14) of various molecular characteristics (see Table 4.1) were synthesized with two different metallocene catalyst

systems. Resins sPP#9 to sPP#11 were synthesized with (isopropylidene(cyclopentadienyl)(9-fluorenyl)zirconiumdichloride) using MMAO as the activator (with the Al/Zr ratio being 2000) in bulk monomer at 70, 50, and 30°C, respectively. Resins sPP#12 to sPP#14 were synthesized with (diphenylmethylidene(cyclopentadienyl)(9-fluorenyl)zirconiumdichloride) using MMAO as the activator (with the Al/Zr ratio being 2000) in bulk monomer at 70, 50, and 30°C, respectively. The as-polymerized polymers were deashed via a solvent/non-solvent liquid–liquid extraction and subsequently stabilized with an antioxidant. The deashed/stabilized polymers were characterized for their molecular weight averages using size-exclusion chromatography (SEC) and their tacticity using ^{13}C-nuclear magnetic resonance (NMR) and the results are summarized in Table 4.1.

Table 4.1 Molecular characteristics of sPP# 9-14 and the equilibrium melting temperature (T_m^0) based on linear and nonlinear Hoffman-Weeks extrapolation

Resin	Mw	Mw/Mn	Racemic dyad	Racemic pentad
			[%r]	[%rrrr]
sPP#9	99,000	2.1	90.8	78.0
sPP#10	136,000	2.2	91.9	80.3
sPP#11	188,000	2.3	92.5	83.0
sPP#12	407,000	3.3	91.4	78.9
sPP#13	606,000	3.2	92.8	83.4
sPP#14	952,000	2.5	95.1	87.8

Resin	Triad Analysis of Data			T_m^0 (°C)	
	%isotactic	%atactic	%syndiotactic	LHW	NLHW
sPP#9	3.3	8.3	88.4	144.2	179.7
sPP#10	2.2	7.9	89.9	156.0	191.7
sPP#11	2.3	7.3	90.4	159.7	193.5
sPP#12	2.6	7.7	89.7	142.3	174.9
sPP#13	2.2	7.0	90.8	151.1	182.7
sPP#14	1.2	5.2	93.6	157.0	189.6

4.4.2 Sample Preparation

The as-polymerized resins were compressed into films by placing the resins between a pair of transparency films, which were later sandwiched between a pair of stainless steel platens in a Wabash V50H compression press. The thickness of the films was 100±10 μm. After being pre-heated at 190°C for 2 min, the films were melt-pressed at 190°C for another 2 min under an applied clamping force of 5 tons. The compression-molded films were then cooled to 40°C in the compression press. The cooling of the platens was achieved by running cold water through channels in the press platens and was fitted well by an exponential decay with a time constant of 3 min.

4.4.3 Differential Scanning Calorimetry Measurements

A Perkin-Elmer Series 7 differential scanning calorimeter (DSC) was used to record isothermal meltcrystallization exotherms and subsequent melting thermograms for these resins. Calibration for the temperature scale was carried out using an indium standard (T_m^0 = 156.6°C and ΔH_f^0 = 28.5 J g^{-1}) on every other run. To minimize thermal lag between the polymer sample and the DSC furnace, each sample holder was loaded with a disc-shaped sample, cut from the asprepared films, and each one weighed around 3.6±0.4 mg. Each sample was used only once and all the runs were carried out under nitrogen atmosphere to minimize thermal degradation.

The experiment started with heating each sample from 25 to 190°C at a heating rate of 80°C min^{-1}, in order to nullify previous thermal history of the sample and to set a standard thermal history to all of the samples studied. To ensure complete melting, each sample was melt-annealed at 190°C for 5 min [16,17] before being quenched to a specified crystallization temperature T_c under a prescribed cooling rate of 200°C min^{-1}. The sample was held at the specified T_c until the crystallization process was considered complete (viz. when no significant change in the heat flow was further observed). The sample was later heated up to 165°C at a heating rate of 20°C min^{-1} in order to observe its subsequent melting behavior. Both the recorded melt-crystallization isotherms and the subsequent melting thermograms were further analyzed accordingly.

4.5 Results and Discussion

4.5.1 Isothermal Melt-Crystallization and Subsequent Melting Behavior

Typical isothermal melt-crystallization exotherms and subsequent melting thermograms for sPP#10 after isothermal crystallization at crystallization temperatures T_c, ranging from 88 to 108°C, are shown in Fig. 4.1. Other sPP resins also showed similar crystallization and melting behavior such as those shown in Fig. 4.1. The main difference in the raw data taken for these different resins was that, due to the difference in the molecular characteristics that these resins exhibit, the observable range of T_c for these resins was essentially different. The difference in the observed T_c range and the difference in the molecular characteristics were responsible for the difference in the crystallization and subsequent melting behavior for these resins.

Fig.4.1(a) shows the typical isothermal melt-crystallization exotherms for sPP#10. For a given exotherm, the heat flow signal started with a fluctuation, a result of the thermal stabilization between the sample and the furnace after the sample was quenched from 190°C down to a specified T_c. The higher the T_c, the shorter the time required for thermal stabilization. If the time required for thermal stabilization did not take longer than the onset of crystallization, the heat flow signal would appear to be similar to those shown in Fig.4.1(a). After thermal stabilization, the heat flow signal, upon crystallization, exhibited an exotherm, a result of the thermal energy released during crystallization, and, after the completion of the crystallization process, the heat flow signal reverted to a normal baseline. The onset of crystallization was determined from the point where a line drawn in parallel to the normal baseline intersects with the heat flow signal. Once the onset of crystallization was determined, each crystallization isotherm was then further analyzed for the crystallization kinetics, which are subjects of subsequent subsections.

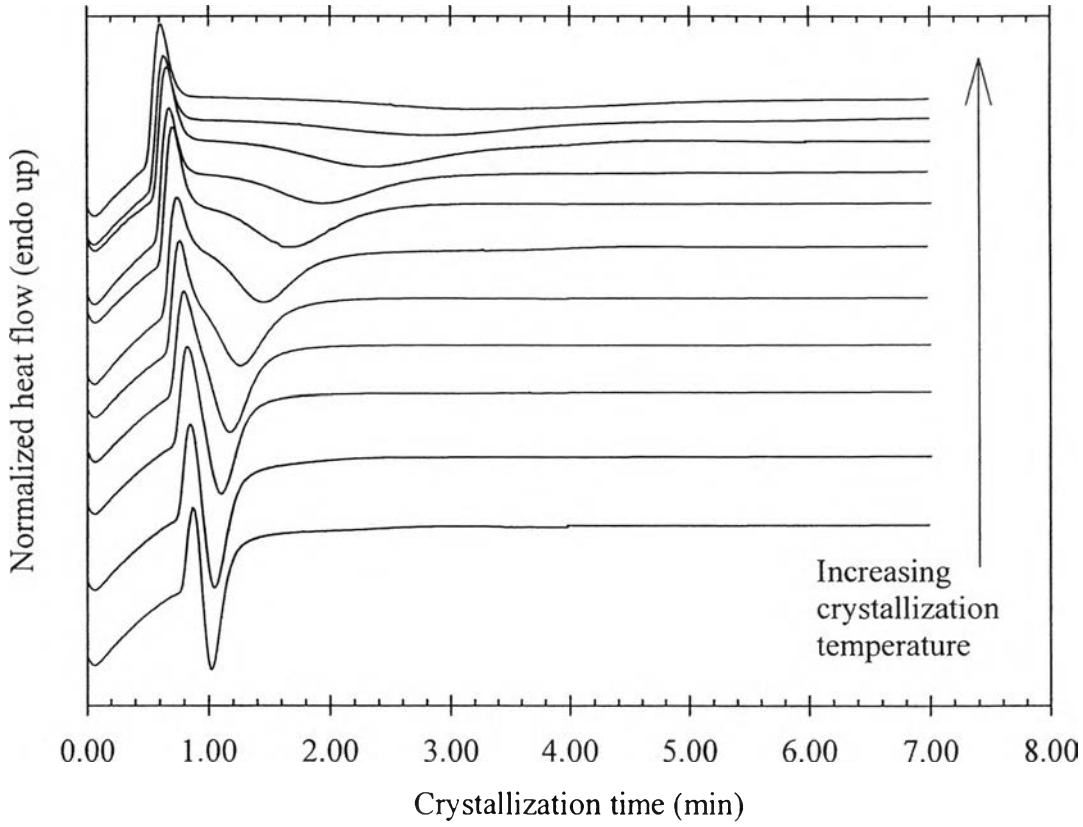

Figure 4.1(a) Isothermal melt-crystallization exotherms for sPP#10 observed at different crystallization temperatures, ranging from 88 to 108°C.

Fig.4.1(b) shows the subsequent melting thermograms for sPP#10 after isothermal melt-crystallization at specified T_c's. The heating rate used to record these curves was 20°C min^{-1}. Either one or two major melting endotherms were clearly visible in these thermograms. For sPP#10, double-melting endotherms were obtained when the T_c was lower than ca.100°C and the single melting endotherm was observed when T_c was greater than ca.100°C. For double melting endotherms, the low-temperature melting endotherm appeared to be more pronounced and shifted towards a higher temperature with increasing T_c (i.e., for sPP#10, from ca.131°C for T_c of 88°C to ca.138°C for T_c of 108°C), while the high-temperature melting endotherm was not much affected by

changes in the T_c. Other resins also exhibited a similar behavior to what has been described for sPP#10. Again, the difference in the molecular characteristics of these resins resulted in the difference in the observed T_c range, hence the difference in the peak position of the melting endotherm(s) observed. Table 4.2 summarizes the observable crystallization range and the peak temperatures of the low- and the high-temperature melting endotherm (i.e. denoted T_{ml} and T_{mh}, respectively) for all of the resins studied.

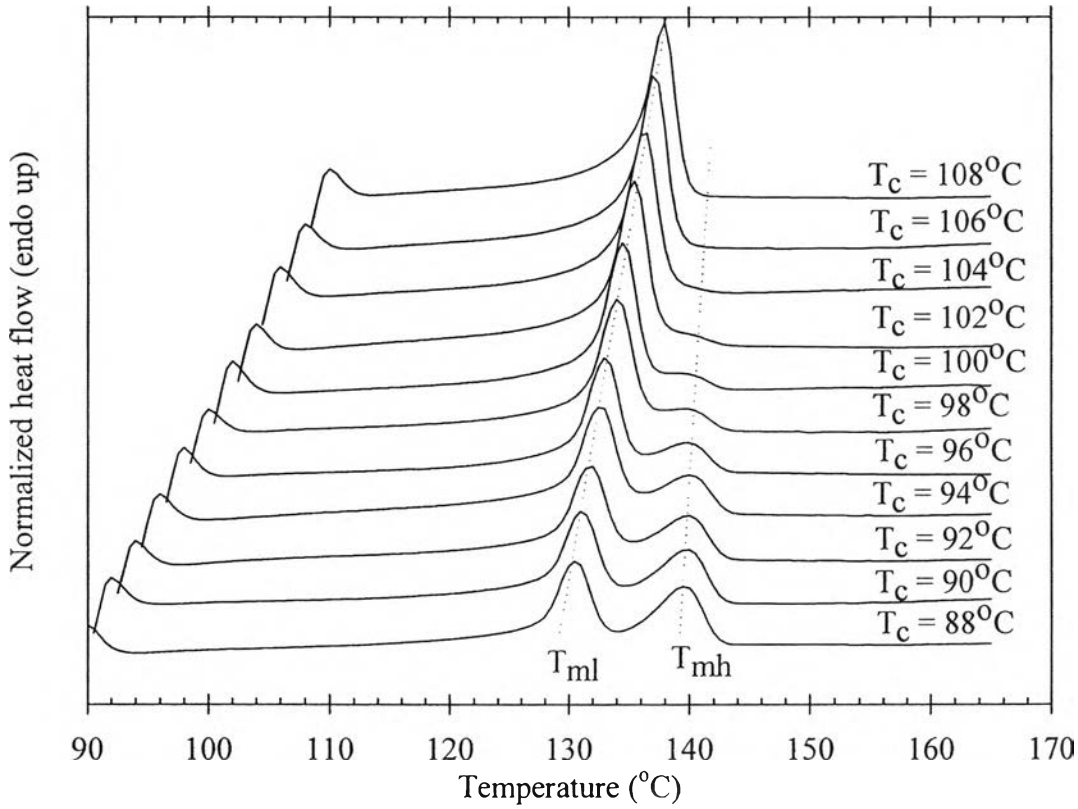

Figure 4.1(b) Subsequent melting thermograms for sPP#10 observed during subsequent heating at a heating rate of 20°C min^{-1} after isothermal melt-crystallization at different crystallization temperatures, ranging from 88 to 108°C.

Table 4.2 Characteristic data of the melting endotherm after isothermal crystallization of sPP# 9-14

sPP#9			sPP#10			sPP#11		
T_c (°C)	T_{ml} (°C)	T_{mh} (°C)	T_c (°C)	T_{ml} (°C)	T_{mh} (°C)	T_c (°C)	T_{ml} (°C)	T_{mh} (°C)
72	118.7	131.0	88	130.7	139.7	90	138.0	145.7
75	119.1	131.1	90	131.0	140.0	92	138.0	145.7
80	121.0	131.7	92	131.7	140.0	94	138.7	145.4
82	121.4	132.0	94	132.7	140.4	96	139.4	145.7
84	122.0	132.0	96	133.0	140.0	98	140.0	146.0
85	122.1	132.1	98	134.0	140.4	100	140.4	145.7
86	122.7	132.4	100	134.7	140.4	102	141.4	-
88	123.4	132.7	102	135.4	-	104	142.0	-
90	124.0	132.4	104	136.4	-	106	142.7	-
92	125.0	133.0	106	137.4	-	108	143.4	-
94	126.0	133.0	108	138.0	-	110	144.0	-
95	126.4	133.1						
98	127.7	133.7						
sPP#12			sPP#13			sPP#14		
T_c (°C)	T_{ml} (°C)	T_{mh} (°C)	T_c (°C)	T_{ml} (°C)	T_{mh} (°C)	T_c (°C)	T_{ml} (°C)	T_{mh} (°C)
74	120.4	129.7	86	130.4	137.0	90	136.7	-
76	120.7	129.4	88	130.7	137.0	92	137.0	-
78	121.4	129.7	90	131.4	-	94	137.7	-
80	121.7	129.7	92	131.7	-	96	138.4	-
82	122.7	130.0	94	132.4	-	98	138.4	-
84	123.0	129.7	96	133.0	-	100	139.0	-
86	123.7	129.7	98	133.7	-	102	139.4	-
88	124.7	130.4	100	134.7	-	104	140.4	-
90	125.4	-	102	135.0	-	106	141.0	-
92	125.7	-	104	136.0	-	108	142.4	-
94	126.7	-	106	136.7	-	110	143.0	-
96	127.4	-						

The multiple melting behavior of sPP has been investigated and reported in a previous publication [18]. The low-temperature melting endotherm was found to associate with the melting of the primary crystallites formed at a T_c, while the high-temperature melting endotherm was attributed to the melting of recrystallized crystallites formed during a subsequent heating scan from the corresponding T_c. In light of this, all of the T_{ml} values summarized in Table 4.2 are associated with the melting (peak) temperature of the primary crystallites formed at each corresponding T_c. These T_{ml} values were to be analyzed to determine the equilibrium melting temperature T_m^0 for each resin.

4.5.2 Determination of Equilibrium Melting Temperature

As mentioned previously, the equilibrium melting temperature T_m^0 is an important thermodynamic parameter for determining the degree of undercooling which signifies the thermodynamic driving force for crystallization of a crystallizable polymer. From the relationship between the observed melting temperature (i.e. T_{ml} in this case) and the crystallization temperature T_c, two extrapolative methods can be used: (1) the linear Hoffman–Weeks (LHW) [15] and (2) the non-linear Hoffman–Weeks (NLHW) [14], respectively.

Fig. 4.2 illustrates the relationship between the Tml and the Tc values for sPP#9. The T_m^0 value based on the LHW method (i.e. T_m^{LHW}) can be determined from the intersect between a linear regression line drawn through the bulk of the T_{ml}–T_c data (i.e. the dotted line) and the $T_m = T_c$ line (i.e. the thick solid line). According to this procedure, the T_m^{LHW} value for sPP#9 was determined to be ca.144.2°C. The T_m^{LHW} values for all of the sPP resins investigated are summarized in Table 1 and, qualitatively, were found to lie in the following order: sPP#11 > sPP#14 > sPP#10 > sPP#13 > sPP#9 > sPP#12.

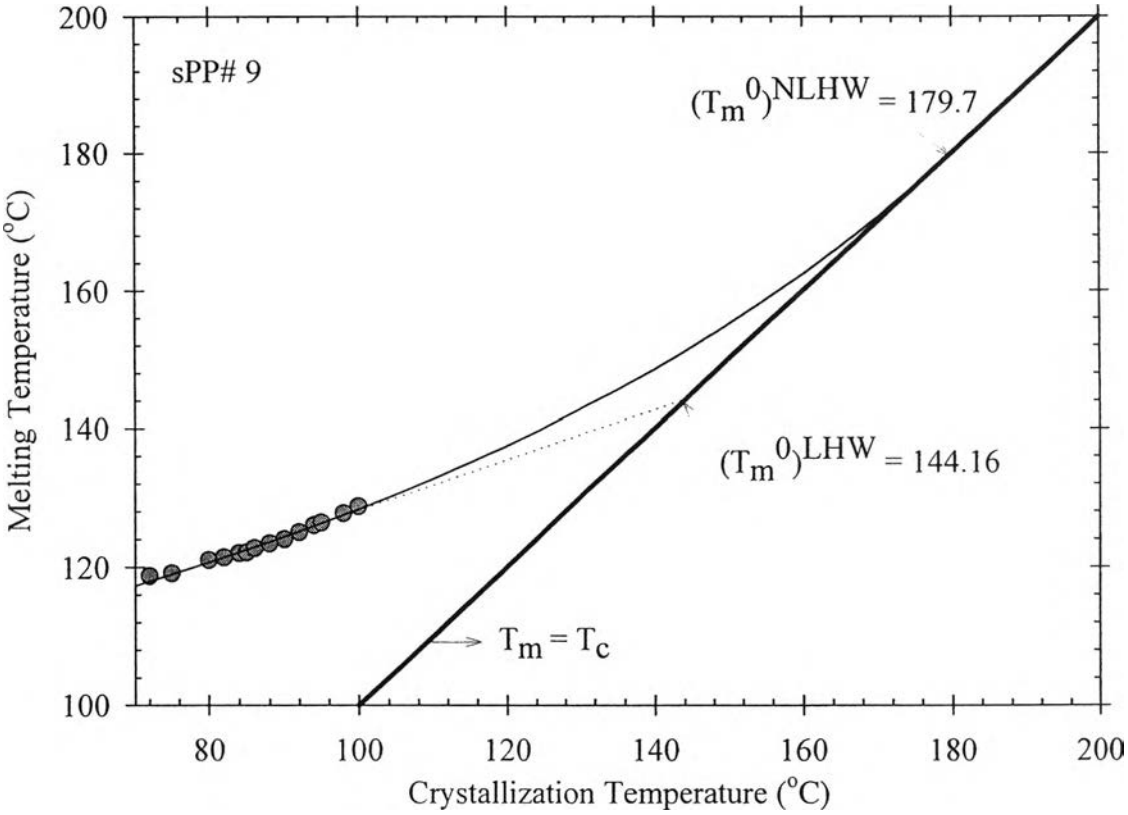

Figure 4.2 Observed melting temperature as a function of crystallization temperature for sPP#9. The raw data are shown as geometrical points. The dotted line represents the linear Hoffman-Weeks extrapolation and the solid line represents the non-linear Hoffman-Weeks extrapolation.

The LHW method predicts that the T_m–T_c data should be linear, and Fig. 4.2 clearly shows slight curvature in the experimental T_{ml}–T_c data, indicating that the LHW model may not be the appropriate model to determine the T_c value for this polymer. By taking a consideration of stem length fluctuation during chain folding [19], the original LHW theory was expanded to the NLHW theory [14], which is able to predict the slight curvature of the observed T_m–T_c data. To use the NLHW method, Eq.(4.6) is rewritten in a much simpler form:

$$M = \beta^m \frac{\sigma_e^1}{\sigma_e^{GT}}(X + a), \tag{4.7}$$

where M, X, and a are reduced parameters. Normally, it is logical to assume that $\sigma_e^{GT} \approx \sigma_e^1$ [14]. In order to apply Eq.(4.7), the reduced parameters M and X have to be calculated from a set of the observed T_m–T_c data, such as those summarized in Table 4.2 for all of the sPP resins investigated, based on an initial guess value of T_m^0. The true T_m^0 value is the guessed T_m^0 value which results in the slope of the M–X plot of 1 (i.e., $\beta^m = 1$). According to this procedure, the T_m^{NLHW} value for sPP#9 was determined to be ca. 179.7°C, with the NLHW prediction is shown as solid line in Fig. 4.2. The T_m^{NLHW} values for all of the sPP resins investigated are summarized in Table 4.1 and, qualitatively, were found to lie in the following order: sPP#11 > sPP#10 > sPP#14 > sPP#13> sPP#9 > sPP#12.

It is clear from the estimated T_m^0 values reported in Table 4.1 that they were found to depend much stronger on the syndiotacticity level than on the molecular weight. Two data sets are clearly observed, with one being those synthesized by (isopropylidene(cyclopentadienyl)(9-fluorenyl)zirconium dichloride) (i.e. sPP#9 to sPP#11) and the other by (diphenylmethylidene(cyclopentadienyl)(9-fluorenyl)zirconium dichloride) (i.e. sPP#12 to sPP#14). Within each set, the estimated T_m^0 values were all found to increase with increasing syndiotacticity level. Comparison of these T_m^0 values (due to the availability of the data in the literature, this would be discussed in terms of the T_m^{NLHW} values only) with those reported in the literature [20] clearly shows that the T_m^0 value is indeed a strong function of the syndiotacticity level. Fig.4.3 illustrates variation of the T_m^0 values (based on the T_m^{LHW} values only) reported in this work (see Table 4.1) and those reported in the literature [20] as a function of the racemic pentad content [%rrrr]. Based on this type of plot [21], the T_m^0 value for a

perfect sPP (i.e. sPP of 100% syndiotacticity level) was estimated to be 173.8°C (with the r^2 parameter being 0.812).

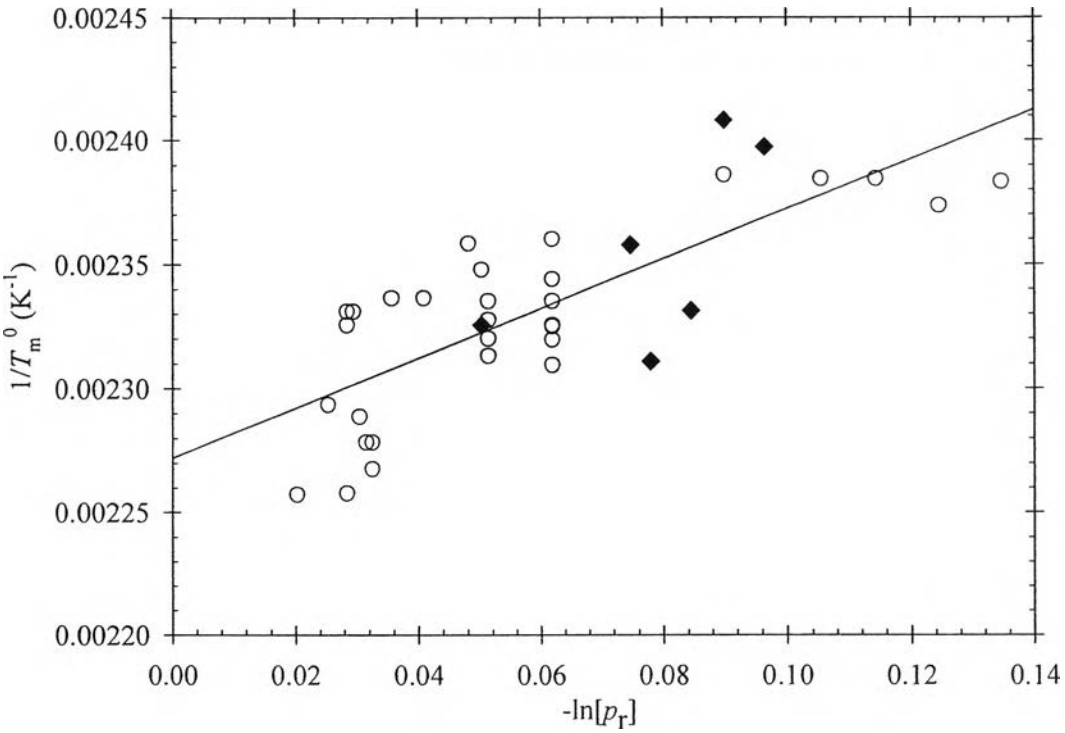

Figure 4.3 Determination of the equilibrium melting temperature for a perfect sPP (i.e. sPP of 100% syndiotacticity level) by extrapolation of the observed equilibrium melting temperatures (i.e. T_m^{LHW}) of the sPP resins shown in Table 4.1 as a function of the racemic pentad content. Keys: data obtained from this work (•) and from the literature (o).

An alternative way for estimating the T_m^0 value for a perfect sPP is to apply a modified Flory's theory for the depression of the T_m^0 value of a random copolymer [22], which states a relationship between the T_m^0 value of a random copolymer and the average mole fraction of the monomer unit present in the copolymer molecules: that is

$$\frac{1}{T_m^0} = \frac{1}{\left(T_m^0\right)_{100\%}} - \left(\frac{R}{\Delta H_f^0}\right) \ln p_r, \tag{4.8}$$

where T_m^0 and $\left(T_m^0\right)_{100\%}$ are the T_m^0 values of a random copolymer and a perfect homopolymer, respectively, ΔH_f^0 is the enthalpy of fusion for a perfect homopolymer, R is the universal gas constant, and p_r is the mole fraction of monomer unit present in the copolymer molecules.

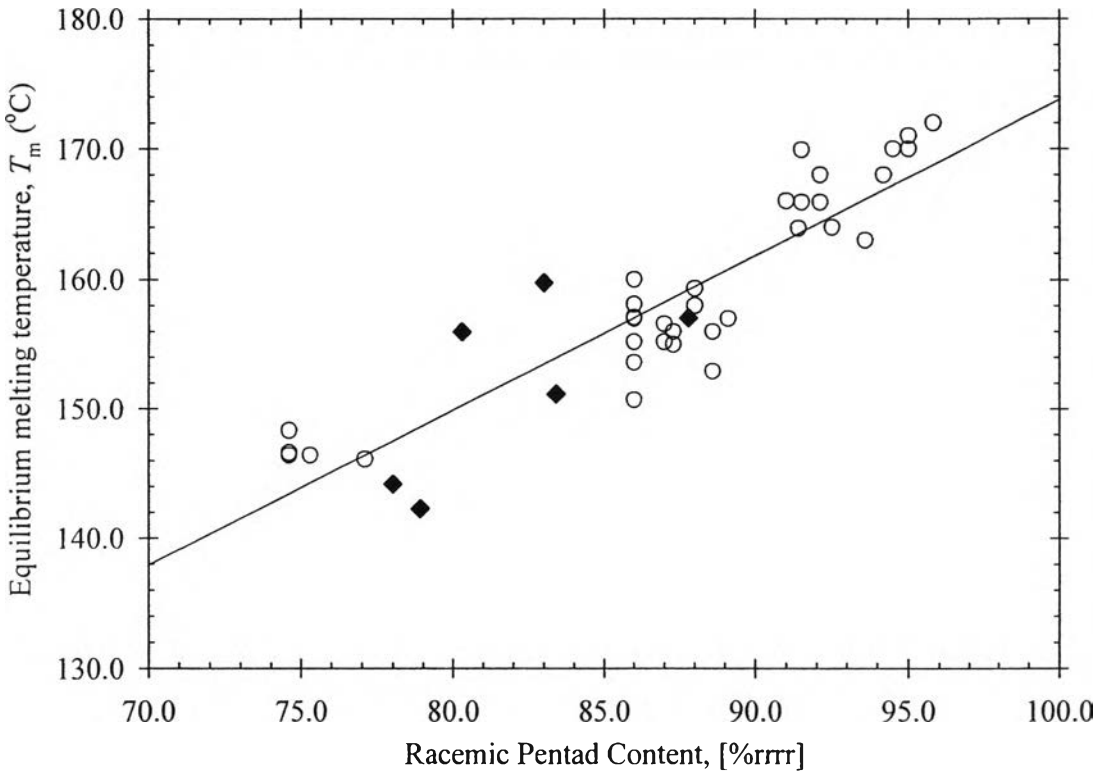

Figure 4.4 Determination of the equilibrium melting temperature for a perfect sPP by means of a modified Flory's theory for the depression of the equilibrium melting temperature in copolymers through the plot of $1/T_m^{LHW}$ versus $-\ln p_r$, where p_r is the racemic dyad content. Keys: data obtained from this work (•) and from the literature (o).

In general, synthesis of a perfect sPP can hardly be achieved. Most available sPP resins can, therefore, be considered as a copolymer, having a certain amount of meso mis-insertions as comonomer unit. In this case, pr can be replaced by the racemic dyad content [%r]. Based on this assumption, the inversed T_m^0 values (based on the T_m^{LHW} values only) reported in this work (see Table 4.1)and those reported in the literature [20] can be plotted as a function of $-\ln(p_r)$ (see Fig. 4.4), from which the T_m^0 and the ΔH_f^0 values for a perfect sPP were estimated to be ca. 167.0°C and 8.3 kJ mol^{-1}, respectively.

4.5.3 Overall Isothermal Melt-Crystallization Kinetics

Based on the typical isothermal melt-crystallization exotherms such as those shown for sPP#10 in Fig. 4.1(a), further analysis of the experimental results can be carried out by transforming the obtained crystallization exotherms into the time-dependent relative crystallinity function $\theta(t)$ such as those shown for sPP#11 in Fig.4.5 (viz.the experimental data are shown as various geometrical points). From these $\theta(t)$ functions, an important kinetic parameter, i.e. the half-time of crystallization $t_{0.5}$ (defined as the elapsed period from the beginning of the crystallization process to a point where 50% of the relative crystallinity is reached), can be obtained. The reciprocal value of the half-time of crystallization, i.e. the reciprocal crystallization half-time $t_{0.5}^{-1}$, is a parameter signifying the overall crystallization rate. Fig. 4.6 illustrates the $t_{0.5}^{-1}$ values for all of the sPP resins studied. Again, two sets of data are obvious: the first is the set of sPP#9, sPP#10, and sPP#11 and the second is the set of sPP#12, sPP#13, and sPP#14, respectively. Within each set, sPP resin with a higher syndiotacticity level was found to have a higher overall crystallization rate (for a given T_c), or, in other words, sPP resin with a higher syndiotacticity level crystallizes faster than sPP resin with a lower syndiotacticity level.

Apart from a direct observation of the overall crystallization kinetics through the analysis of the $t_{0.5}$ and its reciprocal values, the $\theta(t)$ functions can be further

analyzed based on various macrokinetic crystallization models, e.g. the Avrami [i.e. Eq. (4.1)], Malkin [i.e. Eq.(4.3)], and Urbanovici–Segal [i.e. Eq. (4.4)].

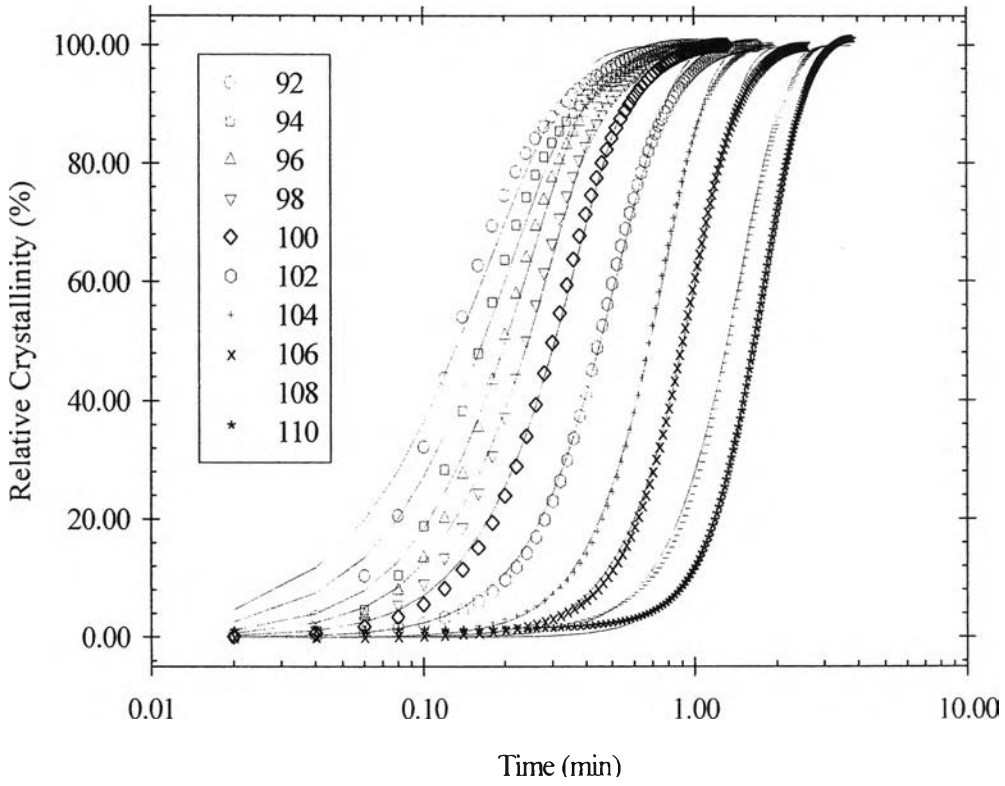

Figure 4.5(a) Relative crystallinity as a function of crystallization time for sPP#11 observed at different crystallization temperatures, ranging from 92 to 110°C. The experimental data, shown as various geometrical points, were fitted to the Avrami macrokinetic models, in which the best fits are shown as solid lines.

4.5.3.1 Avrami Analysis

Data analysis based on the Avrami model can be carried out by fitting the $\theta(t)$ functions such as those shown in Fig.4.5 to Eq.(4.1). Table 4.3 summarizes values of the Avrami kinetic parameters (i.e. the Avrami crystallization rate constant K_A and the Avrami exponent n_A) and values of the r^2 parameter signifying the

quality of the fitting.According to the values of the r^2 parameter shown, the Avrami model seems to the fit the experimental $\theta(t)$ data quite well (cf. the predicted curves based on the Avrami model, shown in Fig. 4.5(a) as the solid lines, versus the experimental data, shown in Fig. 4.5(a) as various geometrical points). For a given resin, K_A was found to decrease with increasing T_c, a characteristic feature of the crystallization in the nucleation-controlled region. Comparison of the K_A values for these resins suggests that the overall crystallization rates of these resins can be qualitatively ranked as the following: sPP#11 > sPP#14 > sPP#10 > sPP#13 > sPP#9sPP#12. Unlike K_A, n_A was found, in general, to increase with increasing T_c. Specifically, the n_A values were found to range from ca. 2.1 to 3.3 for sPP#9, from ca. 1.2 to 3.0 for sPP#10, from ca. 1.4 to 3.2 for sPP#11, from ca. 1.9 to 3.0 for sPP#12, from ca. 1.4 to 2.8 for sPP#13, and, finally, from ca. 1.7 to 2.8 for sPP#14, respectively.

Table 4.3 Isothermal crystallization kinetic parameters of sPP# 9-14 based on Avrami analysis

sPP#9				sPP#10			
T_c (°C)	K_a (min^{-1})	n_a	r^2	T_c (°C)	K_a (min^{-1})	n_a	r^2
75	4.85	2.11	0.9944	88	5.16	1.74	0.9969
80	2.51	2.43	0.9997	90	3.82	1.19	0.9886
82	1.93	2.17	0.9979	92	3.45	2.02	0.9981
84	1.84	2.62	0.9998	94	2.82	2.04	0.9987
85	1.66	2.65	0.9998	96	2.07	2.17	0.9992
86	1.51	2.67	0.9998	98	1.58	2.40	0.9994
88	1.34	2.72	0.9999	100	1.07	2.68	0.9998
90	1.09	2.67	0.9999	102	0.81	2.96	0.9997
92	0.77	3.25	0.9999	104	0.55	2.62	0.9990
94	0.59	3.16	1.0000	106	0.53	2.80	1.0000
95	0.51	3.16	0.9999	108	0.40	2.74	0.9999
98	0.45	2.81	0.9996				
100	0.47	2.67	0.9996				

Table 4.3 Isothermal crystallization kinetic parameters of sPP# 9-14 based on Avrami analysis (*continued*)

sPP#11				sPP#12			
T_c (°C)	K_a (min^{-1})	n_a	r^2	T_c (°C)	K_a (min^{-1})	n_a	r^2
92	5.68	1.40	0.9918	74	3.94	2.09	0.9988
94	4.72	1.53	0.9928	76	3.70	1.98	0.9981
96	4.03	1.75	0.9966	78	3.37	1.91	0.9992
98	3.37	1.84	0.9978	80	2.85	2.01	0.9994
100	2.72	2.01	0.9987	82	2.30	2.26	0.9995
102	1.87	2.20	0.9990	84	1.90	2.38	0.9998
104	1.27	2.66	0.9995	86	1.50	2.62	0.9998
106	0.96	2.71	0.9993	88	1.20	2.75	0.9998
108	0.66	2.73	0.9997	90	1.05	2.68	0.9997
110	0.53	3.18	0.9995	92	0.74	3.03	0.9998
				94	0.66	2.82	1.0000
				96	0.46	3.03	1.0000
sPP#13				sPP#14			
T_c (°C)	K_a (min^{-1})	n_a	r^2	T_c (°C)	K_a (min^{-1})	n_a	r^2
88	3.99	1.78	0.9977	90	5.37	1.73	0.9961
90	3.76	1.61	0.9960	92	5.01	1.89	0.9975
92	2.77	1.44	0.9950	94	3.49	1.90	0.9971
94	2.35	2.01	0.9986	96	2.87	2.14	0.9983
96	1.77	2.06	0.9990	98	2.24	2.42	0.9994
98	1.33	2.13	0.9990	100	1.82	2.39	0.9994
100	1.12	2.29	0.9994	102	1.50	2.58	1.0000
102	0.70	2.84	0.9999	104	1.00	2.79	0.9999
104	0.52	2.82	0.9998	106	0.80	2.43	0.9997
106	0.34	2.55	0.9997	108	0.49	2.80	0.9996
				110	0.32	2.38	0.9984

4.5.3.2 Malkin Analysis

Data analysis based on the Malkin model can be carried out by fitting the $\theta(t)$ functions such as those shown in Fig.4.5 to Eq.(3).Table 4.4 summarizes values of the Malkin kinetic parameters (i.e. the Malkin crystallization rate constant C_1 and the Malkin exponent C_0) and values of the r^2 parameter signifying the quality of the fitting. According to the values of the r^2 parameter shown, the Malkin model seems to provide a fair fitting to the experimental data (cf. the predicted curves based on the Avrami model, shown in Fig. 4.5(b) as the solid lines, versus the experimental data, shown in Fig. 4.5(a) as various geometrical points). For a given resin, C_1 was found to decrease with increasing T_c. Comparison of the C_1 values for these resins suggests that the ranking for the overall crystallization rates of these resins is essentially similar to what has been found by comparing the K_A values. Similarly to n_A, C_0 was also generally found to increase with increasing T_c. Specifically, the C_0 values were found to range from ca. 14.0 to 119.2 for sPP#9, from ca. 0.9 to 73.0 for sPP#10, from ca. 1.9 to 100.4 for sPP#11, from ca. 9.7 to 79.1 for sPP#12, from ca. 2.7 to 59.3 for sPP#13, and, finally, from ca. 7.2 to 55.6 for sPP#14, respectively. Similarity in the behavior of the Malkin kinetic parameters to that of the Avrami ones is not surprising since these parameters are, in fact, related (i.e. $C_0 = 4^{n_A} - 4$ and $C_1 = \ln\left(4^{n_A} - 2\right)\left[K_A/(\ln 2)^{1/n_A}\right]$) [12].

4.5.3.3 Urbanovici-Segal Analysis

Data analysis based on the Urbanovici–Segal model can be carried out by fitting the $\theta(t)$ functions such as those shown in Fig. 4.5 to Eq.(4.4). Table 4.5 summarizes values of the Urbanovici–Segal kinetic parameters (i.e. the Urbanovici–Segal crystallization rate constant K_{US}, the Urbanovici–Segal exponent n_{US}, and the parameter r) and values of the r^2 parameter.According to the values of the r^2 parameter shown, the Urbanovici–Segal model appears to provide an excellent fit to the experimental data (cf. the predicted curves based on the Urbanovici–Segal model, shown in Fig. 4.5(c) as the solid lines, versus the experimental data, shown in Fig. 4.5(c) as various geometrical points). For a given resin, K_{US} was found to correspond to T_c in a similar manner with K_A and C_1. Comparison of the K_{US} values for these resins suggests

that the ranking for the overall crystallization rates of these resins is essentially similar to what has been found by comparing the K_A and C_1 values.Unlike n_A and C_0, n_{US} was not found to hold a specific relationship with T_c. Specifically, the n_{US} values were found to range from ca. 2.5 to 3.5 for sPP#9, from ca. 2.5 to 3.3 for sPP#10, from ca. 2.5 to 3.7 for sPP#11, from ca. 2.3 to 3.8 for sPP#12, from ca. 2.3 to 3.0 for sPP#13, and, finally, from ca. 2.6 to 3.1 for sPP#14, respectively.

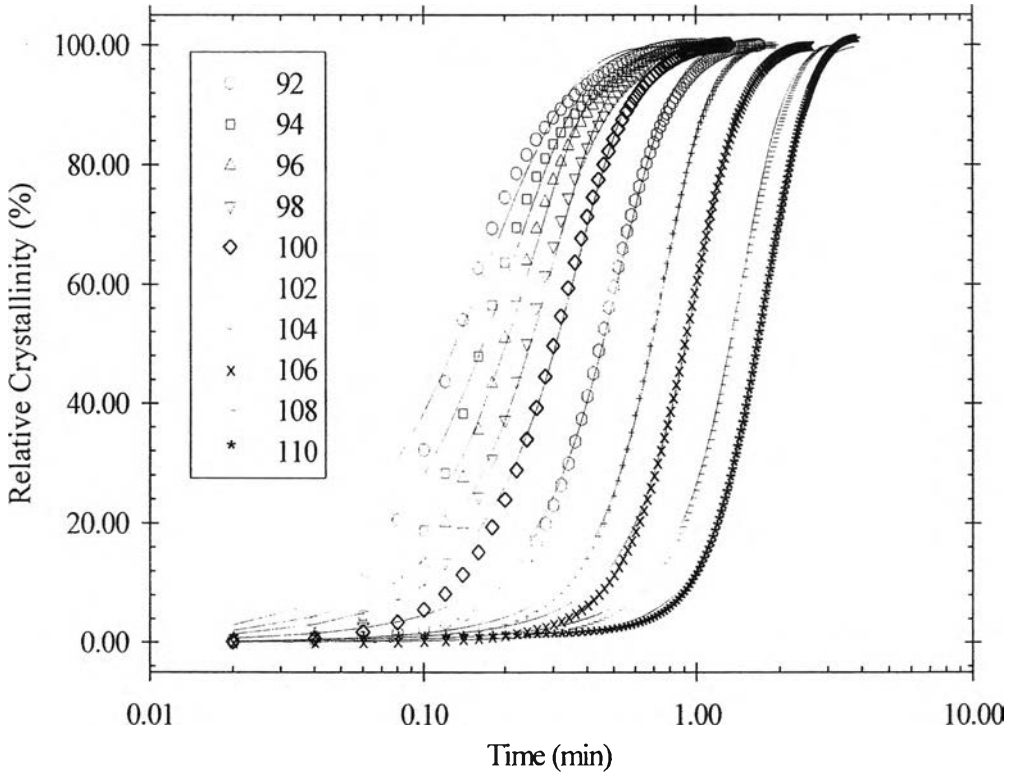

Figure 4.5(b) Relative crystallinity as a function of crystallization time for sPP#11 observed at different crystallization temperatures, ranging from 92 to 110°C. The experimental data, shown as various geometrical points, were fitted to the Malkin macrokinetic models, in which the best fits are shown as solid lines.

Table 4.4 Isothermal crystallization kinetic parameters of sPP# 9-14 based on Malkin analysis

sPP#9				sPP#10			
T_c (°C)	C_1 (min^{-1})	C_0	r^2	T_c (°C)	C_1 (min^{-1})	C_0	r^2
75	15.99	14.03	0.9944	88	13.27	6.06	0.9961
80	9.79	26.89	0.9998	90	5.46	0.86	0.9875
82	6.68	16.66	0.9979	92	10.95	12.13	0.9980
84	7.81	38.77	0.9999	94	9.14	13.40	0.9985
85	7.15	40.28	0.9999	96	7.13	16.69	0.9991
86	6.58	42.40	0.9999	98	6.07	25.41	0.9993
88	5.89	44.17	0.9999	100	4.76	47.29	0.9999
90	4.75	42.76	0.9999	102	3.97	73.04	0.9999
92	4.16	119.17	0.9999	104	2.41	43.66	0.9989
94	3.06	98.61	0.9998	106	2.44	56.34	0.9998
95	2.66	102.88	0.9999	108	1.81	54.10	0.9996
98	2.06	52.79	0.9993				
100	2.03	40.28	0.9995				
sPP#11				sPP#12			
T_c (°C)	C_1 (min^{-1})	C_0	r^2	T_c (°C)	C_1 (min^{-1})	C_0	r^2
92	10.30	1.87	0.9904	74	13.17	14.61	0.9987
94	10.56	3.81	0.9922	76	11.40	11.12	0.9977
96	10.78	6.77	0.9961	78	10.03	9.74	0.9991
98	9.85	9.40	0.9972	80	9.15	12.68	0.9995
100	8.50	11.56	0.9984	82	8.39	20.51	0.9995
102	6.58	17.98	0.9989	84	7.35	25.95	0.9999
104	5.57	44.27	0.9997	86	6.38	37.95	0.9998
106	4.25	45.98	0.9995	88	5.33	46.36	0.9998
108	3.04	53.58	0.9997	90	4.52	40.57	0.9997
110	2.75	100.36	0.9996	92	3.63	74.75	0.9998
				94	3.09	59.06	0.9998
				96	2.26	79.08	0.9998

Table 4.4 Isothermal crystallization kinetic parameters of sPP# 9-14 based on Malkin analysis (*continued*)

sPP#13				sPP#14			
T_c (°C)	C_1 (min^{-1})	C_0	r^2	T_c (°C)	C_1 (min^{-1})	C_0	r^2
88	10.24	6.14	0.9968	90	14.59	7.21	0.9957
90	8.85	4.61	0.9950	92	14.86	9.46	0.9972
92	5.54	2.71	0.9940	94	10.44	9.80	0.9970
94	7.38	11.68	0.9983	96	9.76	15.54	0.9983
96	5.70	12.92	0.9987	98	8.67	25.68	0.9995
98	4.49	15.32	0.9987	100	7.00	25.25	0.9994
100	4.10	21.17	0.9992	102	6.36	38.42	0.9998
102	3.28	58.93	0.9998	104	4.59	54.66	0.9998
104	2.44	59.27	0.9997	106	3.14	27.43	0.9996
106	1.43	35.50	0.9991	108	2.28	55.60	0.9995
				110	1.27	27.65	0.9979

4.5.3.4 Further Discussion of the Kinetics Results

Fig. 4.7 illustrates variation of various crystallization rate parameters (i.e. $t_{0.5}^{-1}$, K_A, C_1, and K_{US}) against T_c for sPP#12 as a log-linear plot. Clearly, the values of all of these rate parameters were found to decrease with increasing T_c, a characteristic of the crystallization in the nucleation-controlled region. Interestingly, values of $t_{0.5}^{-1}$, K_A, and K_{US} were all found to lie within the same order to magnitude, which were much lower than those of C_1. Comparison of the values of these rate parameters suggest that the crystallization rates of these sPP resins are in the following order: sPP#11 >sPP#14 > sPP#10 > sPP#13 > sPP#9 ≈ sPP#12. We have also reported that the estimated T_m^0 values (based on the T_m^{LHW} values) for all of the sPP resins investigated were found to lie in the following order: sPP#11 > sPP#14 > sPP#10 > sPP#13 >sPP#9 > sPP#12. The ranking of these resins based on the crystallization rates

and the estimated T_m^0 values is attributed more to the difference in the syndiotacticity level, rather than the molecular weight, that these resins exhibit.

Instead of comparing the values of the rate parameters for a given T_c, the values of these rate parameters for a given value of the degree of undercooling ΔT (i.e. $\Delta T = T_m^0 - T_c$, where T_m^0 is the T_m^{LHW} values obtained) were found to be quite comparable. For examples, the Avrami rate constants for these sPP resins (i.e. sPP#9 to sPP#14) at ΔT of 50°C were found to be ca. 0.59, 0.53, 0.53, 0.74, 0.91, and 0.65 min^{-1}, respectively, while the Malkin rate constants were found to be ca. 3.06, 2.44, 2.75, 3.63, 3.69, and 2.71 min^{-1}, respectively, and the Urbanovici–Segal rate constants were found to be ca. 0.59, 0.53, 0.56, 0.77, 0.96, and 0.68 min^{-1}, respectively.

Table 4.5 Isothermal crystallization kinetic parameters of sPP# 9-14 based on Urbanovici-Segal analysis

sPP#9					sPP#10				
T_c (°C)	K_{us} (min^{-1})	n_{us}	r	r^2	T_c (°C)	K_{us} (min^{-1})	n_{us}	r	r^2
75	6.38	3.48	2.31	0.9993	88	6.64	3.22	2.20	0.9995
80	2.66	2.69	1.26	0.9999	90	5.21	2.51	2.14	0.9992
82	2.23	2.79	1.62	0.9997	92	4.02	2.70	1.62	1.0000
84	1.92	2.87	1.21	0.9999	94	3.21	2.61	1.53	0.9999
85	1.73	2.86	1.18	0.9999	96	2.27	2.58	1.38	0.9999
86	1.58	2.91	1.19	0.9999	98	1.71	2.80	1.35	0.9999
88	1.39	2.92	1.18	1.0000	100	1.11	2.93	1.18	0.9999
90	1.13	2.86	1.15	1.0000	102	0.85	3.29	1.23	0.9999
92	0.79	3.44	1.12	1.0000	104	0.59	3.09	1.35	0.9997
94	0.59	3.12	0.98	1.0000	106	0.53	2.77	0.98	1.0000
95	0.52	3.31	1.09	0.9999	108	0.40	2.75	1.00	0.9999
98	0.43	2.51	0.76	1.0000					
100	0.45	2.37	0.81	0.9999					

Table 4.5 Isothermal crystallization kinetic parameters of sPP# 9-14 based on Urbanovici-Segal analysis (*continued*)

sPP#12					sPP#11				
T_c (°C)	K_{us} (min^{-1})	n_{us}	r	r^2	T_c (°C)	K_{us} (min^{-1})	n_{us}	r	r^2
74	4.88	3.84	2.18	0.9981	92	7.94	2.94	2.33	0.9996
76	4.34	2.70	1.68	0.9999	94	6.27	3.08	2.26	0.9997
78	3.77	2.27	1.40	0.9998	96	4.95	2.69	1.83	0.9999
80	3.12	2.34	1.34	0.9998	98	3.95	2.56	1.63	0.9999
82	2.48	2.58	1.32	0.9999	100	3.08	2.52	1.49	0.9999
84	1.98	2.56	1.17	0.9999	102	2.08	2.70	1.45	0.9999
86	1.57	2.87	1.21	1.0000	104	1.35	3.08	1.31	0.9999
88	1.26	3.00	1.21	1.0000	106	1.04	3.20	1.38	0.9999
90	1.11	2.99	1.27	1.0000	108	0.69	2.98	1.17	0.9999
92	0.77	3.30	1.21	1.0000	110	0.56	3.70	1.35	1.0000
94	0.67	2.86	1.02	1.0000					
96	0.45	2.97	0.97	1.0000					
sPP#13					sPP#14				
T_c (°C)	K_{us} (min^{-1})	n_{us}	r	r^2	T_c (°C)	K_{us} (min^{-1})	n_{us}	r	r^2
88	4.86	2.54	1.77	0.9998	90	6.62	2.77	1.87	0.9998
90	4.70	2.66	1.90	0.9999	92	5.96	2.63	1.69	0.9999
92	3.49	2.33	1.78	0.9995	94	4.20	2.64	1.74	0.9998
94	2.67	2.54	1.48	0.9999	96	3.28	2.70	1.56	0.9999
96	1.97	2.51	1.41	0.9999	98	2.42	2.77	1.34	0.9999
98	1.48	2.60	1.41	0.9999	100	1.97	2.77	1.34	0.9999
100	1.20	2.64	1.30	1.0000	102	1.52	2.64	1.05	1.0000
102	0.72	3.02	1.14	1.0000	104	1.02	2.93	1.11	1.0000
104	0.54	3.04	1.15	1.0000	106	0.84	2.66	1.20	1.0000
106	0.35	2.61	1.06	0.9997	108	0.52	3.08	1.22	0.9999
					110	0.36	3.01	1.54	0.9994

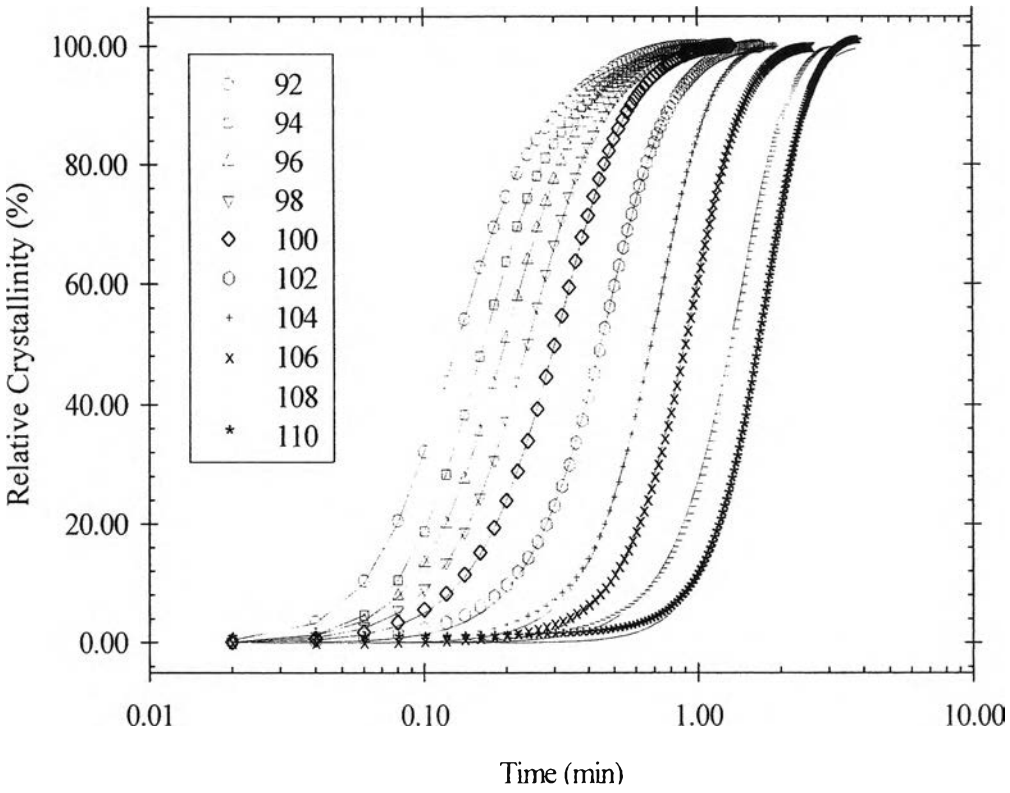

Figure 4.5(c) Relative crystallinity as a function of crystallization time for sPP#11 observed at different crystallization temperatures, ranging from 92 to 110°C. The experimental data, shown as various geometrical points, were fitted to the Urbanovici-Segal macrokinetic models, in which the best fits are shown as solid lines.

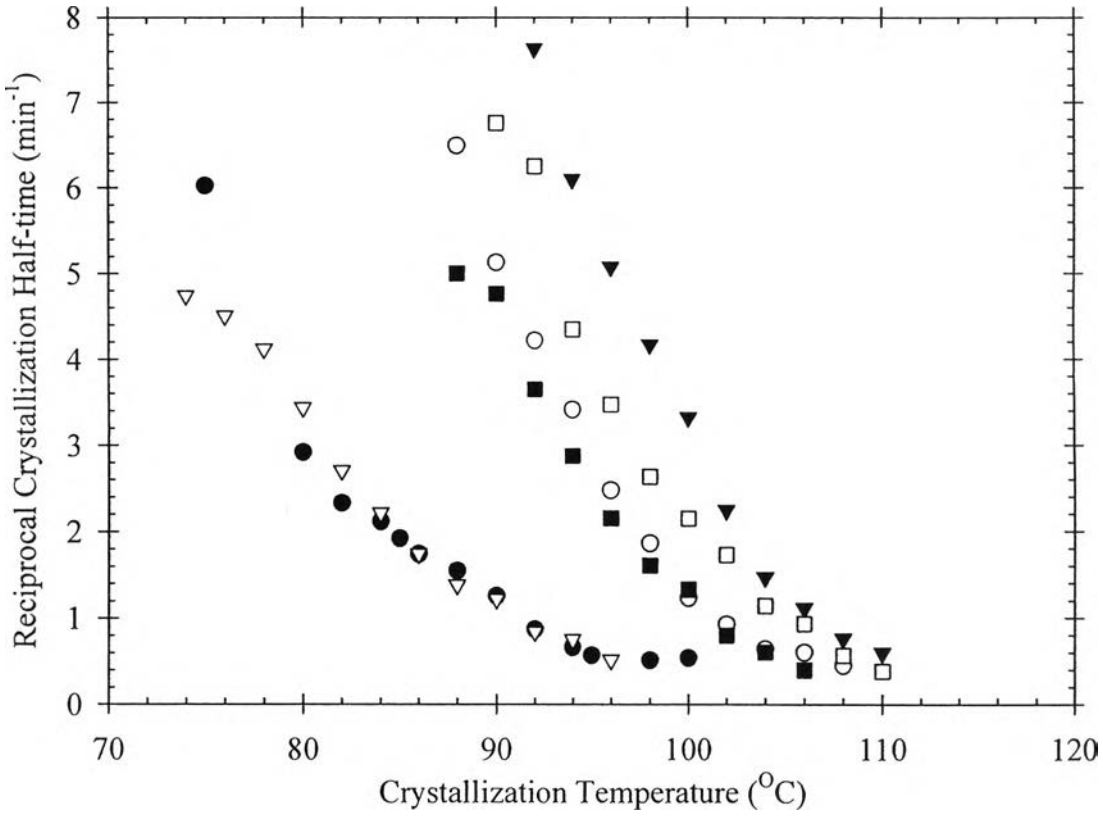

Figure 4.6 Reciprocal half-times of crystallization as a function of crystallization temperature for (●) sPP#9, (○) sPP#10, (▼) sPP#11, (▽) sPP#12, (■) sPP#13, and (□) sPP#14.

4.5.4 Effective Activation Energy Describing the Overall Isothermal Melt-Crystallization Process

Within a small T_c range, the temperature dependence of a crystallization rate parameter can be approximated by an Arrhenius equation. If the Avrami rate constant K_A is used, the effective activation energy describe the overall isothermal melt-crystallization process E_a can be described by the following equation:

$$K_A(T_c) = K_{A,0} \exp[-E_A/RT_c], \tag{4.9}$$

where $K_{A,0}$ is a pre-exponential parameter. Based on Eq. (4.9), the value of E_a, therefore, takes the value of the slope of the plot of $\ln(K_A)$ versus $-1/RT_c$. From the variation of all of the K_A values with T_c as being summarized in Table 4.3, the value of E_a was calculated to be ca. -111.5, -152.5, -160.3, -105.8, -156.2, and -159.0 kJ mol^{-1} for sPP#9 to sPP#14, respectively. Based on these values, the sPP resins investigated can be ranked based on the E_a value from low to high as sPP#11 < sPP#14 < sPP#13 <sPP#10 < sPP#9 < sPP#12. Higher E_a value suggests higher barrier for isothermal melt-crystallization. Therefore, the crystallization ability of these sPP resins based on the E_a values obtained falls in the following order: sPP#11 > sPP#14 > sPP#13 > sPP#10 > sPP#9 > sPP#12.

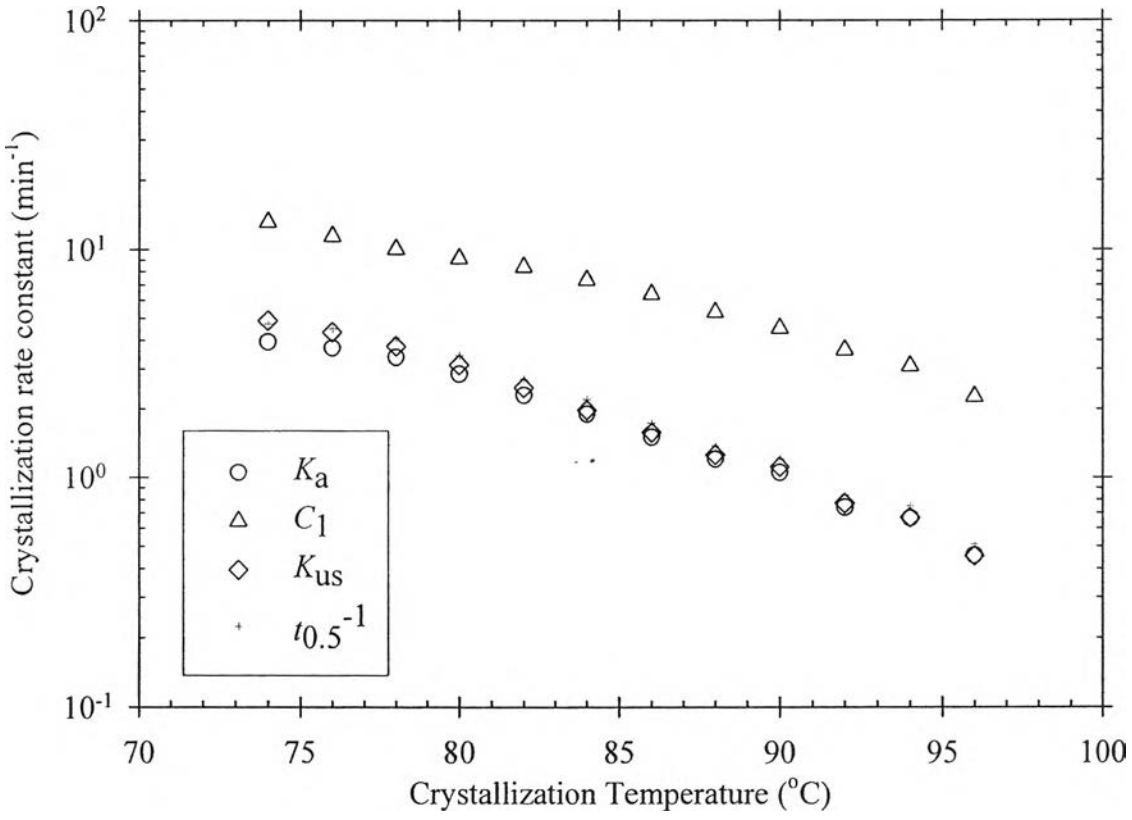

Figure 4.7 Various crystallization rate parameters shown as various geometrical points as a function of crystallization temperature for sPP#12 observed at different crystallization temperatures, ranging from 74 to 96°C.

4.6 Conclusions

In the present contribution, the overall isothermal melt-crystallization and subsequent melting behavior of six metallocene-catalyzed syndiotactic polypropylene (sPP) resins having different molecular characteristics were investigated using differential scanning calorimetry (DSC) technique. Two sets of these sPP resins were synthesized from two different catalyst systems at three different temperatures. The first set contained three resins having the weight-average molecular weight in the range of 99,000 to 188,000 Da and the racemic pentad contents in the range of ca.78 to 83%, while the second set contained three resins having the weight-average molecular weight in the range of 407,000 to 952,000 Da and the racemic pentad contents in the range of ca.79 to 88%.

The overall isothermal melt-crystallization studies revealed that the crystallization rates of these sPP resins depended on the syndiotacticity level rather than on the molecular weight, with sPP resin having higher syndiotacticity level being found to have a higher crystallization rate (for a given crystallization temperature) than that having lower syndiotacticity level. The experimental data were found to be best described by the Urbanovici–Segal model, followed by the Avrami and the Malkin ones, respectively. For a given resin, all of the overall crystallization rate parameters were found to decrease in their values with increasing the crystallization temperature, a characteristic of the crystallization in the nucleation controlled region. Comparison of the bulk crystallization rates of these resins for a given crystallization temperature suggested that the crystallization rates of these resins fell on the following order sPP#11 > sPP#14 > sPP#10 > sPP#13 > sPP#9 sPP#12. Based on the values of the effective activation energy describing the overall isothermal melt-crystallization process estimated for these resins, the crystallization ability of these resins fell on the following sequence: sPP#11 >sPP#14 > sPP#13 > sPP#10 > sPP#9> sPP#12.

Two extrapolative methods, namely the linear and non-linear Hoffman–Weeks, were used to estimate the equilibrium melting temperature T_m^0 for each of these sPP

resins. The estimated T_m^0 values based on the linear Hoffman–Weeks method were found to lie in the following order: sPP#11 > sPP#14 > sPP#10 > sPP#13 > sPP#9 > sPP#12, while those based on the non-linear Hoffman–Weeks method were in the following sequence: sPP#11 > sPP#10 > sPP#14> sPP#13 > sPP#9 > sPP#12. In general, the estimated T_m^0 values were found to increase with increasing syndiotacticity level. By plotting these values along with the values obtained from the literature as a function of the racemic pentad content, the T_m^0 value for a perfect sPP was estimated to be ca. 174°C, and, based on a modified Flory's theory for the depression of the T_m^0 value of a random copolymer, the T_m^0 value for a perfect sPP was, instead, estimated to be ca. 167°C.

4.7 Acknowledgements

This work is supported in parts by the Thailand Research Fund through the Royal Golden Jubilee Ph.D. Program (2.L.CU/45/H.1), the Petroleum and Petrochemical Technology Consortium (through a Thai governmental loan from the Asian Development Bank), and the Petroleum and Petrochemical College, Chulalongkorn University, Thailand.

4.8 References

[1] Natta G, Pasquon I, Corradini P, Peraldo M, Pegorado M, Zambelli A. Rend Acd Naz Lincei 1960;28:539.

[2] Natta G, Pasquon I, Zambelli A. J Am Chem Soc 1962;84:1488.

[3] Ewen JA, Johns RL, Razavi A, Ferrara JD. J Am Chem Soc 1988;110:6255.

[4] Schardl J, Sun L, Kimura S, Sugimoto R. SPE-ANTEC Proc 1995:3414.

[5] Schardl J, Sun L, Kimura S, Sugimoto R. J Plastic Film Sheet 1996;12:157.

[6] Sun L, Shamshoum E, DeKunder G. SPE-ANTEC Proc 1996:1965.

[7] Gownder M. SPE-ANTEC Proc 1995:2275.

[8] Sura RK, Desai P, Abhiraman AS. SPE-ANTEC Proc 1999:1764.

[9] Avrami M. J Chem Phys 1939;7:1103.

[10] Avrami M. J Chem Phys 1940;8:212.

[11] Avrami M. J Chem Phys 1941;9:177.

[12] Malkin AY, Beghishev VP, Keapin IA, Bolgov SA. Polym Eng Sci 1984;24:1369.

[13] Urbanovici E, Segal E.Thermochim Acta 1990;171:87.

[14] Marand H, Xu J, Srinivas S. Macromolecules 1998;31: 8219.

[15] Hoffman JD, Weeks JJ. J Res Natl Bur Stand A 1962;66: 13.

[16] Supaphol P, Spruiell JE. J Appl Polym Sci 2000;75:337.

[17] Supaphol P, Lin JS. Polymer 2001;42:9617.

[18] Supaphol P. J Appl Polym Sci 2001;82:1083.

[19] Lauritzen Jr JI, Passaglia E. J Res Natl Bur Stand A 1967;71:261.

[20] Supaphol P. J Appl Polym Sci 2001;79:1603.

[21] De Rosa C, Auriemma F, Vinti V, Galimberti M. Macromolecules 1998;31:6206.

[22] Miller RL. J Polym Sci 1962;57:975.